Numerical modeling of prestressed fiber reinforced high performance concrete beams subjected to shear

P. Riva & F. Minelli
Department of Civil Engineering, University of Brescia, Italy.

ABSTRACT: Several experimental tests have demonstrated the effectiveness of steel fibers in substituting the minimum code required shear reinforcement in beams, particularly in precast high performance concrete structures. Despite the large number of experimental results available, only a few numerical studies have been so far published concerning fiber reinforced concrete structures. The behavior of full scale steel fiber reinforced concrete beams is herein analysed using a smeared crack damage model provided by the latest release of ABAQUS (V. 6.3). The numerical model is validated against the experimental results obtained on full scale FRC beams. The numerical results allow to correctly predict the experimental response, particularly with respect to the first cracking point, the initial crack pattern, and its development. The results allow a better understanding of fiber reinforced concrete structures under shear loading and will be used as a basis for developing a new design procedure for such kind of structures.

Keywords: Shear loading, fiber reinforced concrete, finite elements analyses.

1 INTRODUCTION

The use of fiber-reinforced high performance concrete (FRHPC) has gained considerable attention in the last few years, particularly when crack propagation control is of primary importance, such as in slab-on-grade applications (Meda et al. 2003) or in beams when shear reinforcement is partly or totally missing (Casanova et al. 1997, Meda et al. 2002). The use of FRHPC in precast industry may become particularly appealing if it will be possible to demonstrate that sufficient strength and ductility may be reached in prestressed beams even in the absence of shear reinforcement.

Numerical modeling of the non-linear behavior of FRHPC materials requires the use of advanced computer codes, which implement material nonlinearities and allow to correctly model concrete fracture phenomena, fundamental when crack development and propagation significantly influence the structural response.

Paramasivan et al. (1995) presented a finite element (FE) formulation for modeling the behavior of partially prestressed steel fiber reinforced concrete (FRC) beams under shear loading. Their formulation treated steel fiber concrete as an ortotropic material characterized by appropriate constitutive relations in the principal compressive and tension directions. The post cracking tensile stress of FRC was related to an orientation factor, a fiber length efficiency factor, the fiber volume fraction and their ultimate bond strength. An experimental program was carried out in order to validate the proposed model, finding that the adopted FE formulation could accurately predict the failure mode and the ultimate load.

Padmarajaiah & Famaswamy (2002) presented an assessment of the flexural behavior of fifteen fully/partially prestressed high strength concrete (HSC) beams containing steel fibers, investigated using 3D non linear FE analysis. Influence of fibers on concrete failure, non linear stress-strain response for HSC, prestressing wire and deformed bar, bond-slip between concrete and reinforcement (fibers, prestressing wires or deformed bars) were also considered in the analyses. A probability approach for predicting the number of fibers per unit cross-sectional area of concrete and their orientation was also implemented. The load-deformation response and the crack patterns obtained from the FE solution were in close agreement with the experimental results, indicating

that the effect of fibers on concrete strength and ductility, and their bridging action in controlling crack propagation, were suitably captured.

In the present work, the results of the non-linear analyses performed on a set of prestressed FRHPC beams subjected to shear, tested at the University of Brescia, are presented. The numerical analyses of the beams were carried out adopting a 3D solid model. The model was developed considering the variation of section along the beam axis, taking into account bond between the prestressing strands and concrete, and modeling the non-linear behavior of the materials. Due to the geometry of the beams, which were designed to fail in shear near one support, only the portion of the beam which was interested by the development of the shear resisting mechanisms was modelled considering material non-linearities, whereas the remaining parts of the beams were considered as linear elastic.

The non-linear analyses of the beams were carried out using the FE program ABAQUS. The analyses allowed to study in detail the development of shear resistant mechanisms in beams with and without shear reinforcement, and allowed to evaluate the relative merits of the FE program adopted.

2 NUMERICAL MODELING

A set of numerical analyses was performed on three high performance concrete beams, having the geometry shown in Figure 1. Two shear tests were carried out on each beam, adopting the layout illustrated in Figure 2. The first test concerned zone TZ (transfer zone), while the second was devoted to zone DZ (diffused prestressing action zone). Tests in TZ zone were representative of the beam behavior near supports, where transverse reinforcement is necessary to improve both the strand bond behavior and the shear strength of the beam, while those in zone DZ represented the behavior in an internal part of the beam, where a minimum reinforcement amount is usually required and the prestressing action is completely diffused.

The test area was 1.75 m long (5 times the web depth) and the beam length was 9 m. The beams were simply supported with a span of 5.65 m and a point load was applied 2.2 m away from support "B" (Fig. 2), thus resulting in a constant shear force along the collapse zone, the dead load being negligible. All beams were designed according to Eurocode 2 (EC2, 1993) provisions in order to have a shear failure in either of the two test zones. For this reason, the web outside of the experimental zones (the collapse location B1 and B2 of Fig.1) was stiffened: the section of the beam along the test zones had therefore the typical geometry of a widespread precast beam with a 120 mm thick web panel.

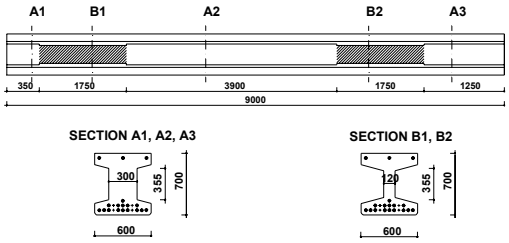

Figure 1. Geometry of the full scale beams.

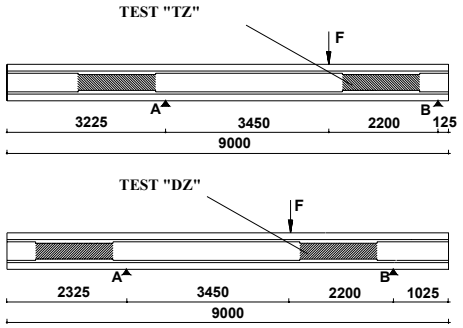

Figure 2. Scheme of the loading phases.

In TZ and DZ zones, different transverse reinforcement amounts were adopted:

- Beam 1 was made of prestressed concrete with transverse reinforcement designed according to EC2 (1993). In TZ zone the stirrups (ϕ6@100 mm) were designed on the basis of the truss mechanism, while in DZ zone transverse reinforcement was the minimum required by the code (welded mesh fabric ϕ5@200x200 mm);
- TZ zone of Beam 2 and Beam 3 (fiber reinforced concrete beams) was made with the same transverse reinforcement of Beam 1. In the same beams, the DZ zone was made without traditional rebars, so that steel fibers were the only reinforcement present in the beam web.

In the remaining parts of the beams stirrups ϕ10@100 mm were adopted. Table 1 summarizes the shear reinforcement adopted in both zones for all the beams tested.

In order to simulate the beams, a solid 3D model was developed. The symmetry of the cross section made possible to model one half of the section, as shown in Figure 3. A 3D model was preferred over a 2D model, as the stress distribution, the crack formation and development might be significantly affected by the abrupt section change. The FE

mesh was made of 9767 first order hexahedral elements and 572 tetrahedral elements.

Table 1. Shear reinforcement in each experimental test.

	TEST	SHEAR REINFORCEMENT (experimental panel)
BEAM 1	TZ	stirrups (design reinf.)
	DZ	Mesh (minimum reinf.)
BEAM 2	TZ	stirrups +45/30 fibers
	DZ	45/30 fibers
BEAM 3	TZ	stirrups +80/30 fibers
	DZ	80/30 fibers

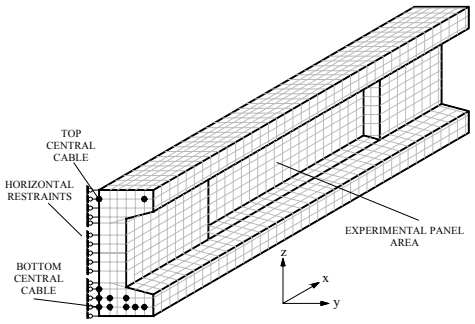

Figure 3. Fe model of the beams.

As far as reinforcement is concerned, different modeling solutions were adopted. Prestressing steel reinforcement (0.6" low-relaxation strands) was modeled by using truss elements, linking nodes having the same coordinates of concrete nodes, but different numbering. In order to evaluate the slip between concrete and prestressing steel, particularly important along the transfer length a set of elastic spring elements was used to link each couple of coincident steel/concrete nodes in the longitudinal direction. The remaining degrees of freedom at the coincident steel/concrete nodes were constrained by means of equations imposing the equality of the transverse displacements. Since the transfer length is usually equal to approximately 80 times the cable diameter (1200 mm in the present case), the spring stiffness was chosen such that the design prestressing force was fully transferred to concrete at a distance of 1200 mm from the beam end. A constant value of k= 50 000 N/mm was thus assumed, leading to the stress distribution in the cables shown in Fig. 4. The stress distribution refers to the structure after all prestressing losses took place and before the shear test.

Deformed bars, which were placed in order to control crack formation and development, and to allow the structure to reach a higher ductility, were modelled by using truss elements, placed between concrete nodes at their correct location. Perfect steel-to-concrete bond was thus assumed.

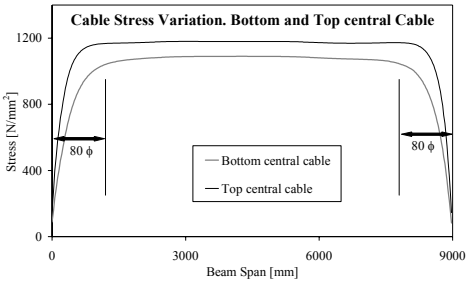

Figure 4. Cable stress variation along the span, Phase II (bottom and top central cables of Fig. 3).

Stirrups and welded wire mesh were modelled using the *REBAR option, which allows users to embed any amount of reinforcement in a mother concrete element. Perfect bond between steel and concrete was assumed also in this case.

Figure 5 depicts the FE mesh. In order to avoid unrealistic punching failure and numerical stability problems due to load concentration, supports and point load were simulated as nodal loads acting on a steel plate 100 mm long (x direction), 300 mm wide (y direction) and 30 mm thick (z direction) connected to the beam. A distributed load was therefore transferred to the concrete structure.

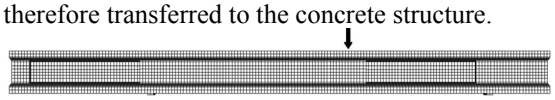

Figure 5. Mesh drawing in the case of DZ test.

A phase analysis was adopted to analyze the beam response during the different loading stages. Three different phases were performed.

- PHASE I: pretension loading applied to the cables, which were the only active elements in the FE model. In order to account for the prestressing losses, a tensile stress of 1190 MPa was applied to all cables instead of the original 1400 MPa, applied during jacking. Loading was applied by means of the *INITIAL CONDITION, TYPE=STRESS option. Finally, the cables were restrained at the ends so that they acted as statically determinate structures;
- PHASE II: concrete casting and cable release. All concrete, spring and rebar elements were activated by means of the *MODEL CHANGE option. Boundary conditions were also modified with the *BOUNDARY, OPT=NEW option: the cable restraints were released and the beam was simply supported, so that the prestressing action

could take place. The cable release loading phase was therefore investigated. The stress along the cable (Fig. 4) was in close agreement with the value predicted by analytical models and the upward displacement was similar to that measured on the actual beams. Figure 6 shows the beam camber at pretensioning. The upward displacement was approximately equal to 2 mm, in the TZ model, at point load location.

- PHASE III: shear test. After applying the new boundary conditions to the structure (different between TZ and DZ tests, as shown in Fig. 2), the point load was increased up to failure.

Figure 6. Beam camber at cable release (Phase II).

3 MATERIAL PROPERTIES

The numerical analyses were performed on specimens made of high performance concrete (HPC). Beam 1 was cast using plain concrete while 50 Kg/m^3 of hooked steel fibers were added to the mix of Beam 2 and Beam 3.

3.1 *Concrete*

Concrete mechanical properties adopted in the numerical analyses, illustrated in Table 2, are based on the results of a number of tests performed on the same mixes used in casting the full scale beams. The tensile strength (f_{ct}) was determined from direct tension tests on cylinders (ϕ=80 mm, l=240 mm), the elastic modulus (E_c) was measured from compression tests on cylinders, and the compressive strength ($f_{c,cube}$) was determined from 150 mm cubes. The cylinder compressive strength f_c was determined from $f_{c,cube}$ according to EC2 (1999). For the Poisson's modulus, a value ν=0.2 was used in all the analyses.

Table 2. Mechanical properties of concrete.

SPECIMEN	$f_{c,cube}$	f_c	f_{ct}	E_c
	MPa	MPa	MPa	MPa
BEAM 1	86.1	71.5	3.69	41 556
BEAM 2	82.3	68.3	4.65	44 191
BEAM 3	92.8	77.0	5.18	43 053

Fibers were 30 mm long. Two different aspect ratio fibers were adopted (aspect ratio l/ϕ *=45* and l/ϕ*=80*): 45/30 fibers had normal strength (1250 MPa), while 80/30 fibers, due to higher hardening, had a higher value of ultimate strength (approximately 2300 MPa).

Based on these material properties, the damaged plasticity model provided in ABAQUS V. 6.3 (HKS, 2002) was adopted. The model is primarily intended to provide a general capability for the analysis of concrete and quasi brittle material structures, mainly failing with cracking in tension and crushing in compression. It aims to capture the effects of irreversible damage associated with failure mechanisms. The main features of the model are: different yield strengths in tension and compression; softening behavior in tension as opposed to initial hardening followed by softening in compression; different degradation of the elastic stiffness in tension and compression; stiffness recovery effects during cyclic loading, and rate sensitivity (especially an increase of peak strength with strain rate). Damaged states in tension and compression are characterized independently by two hardening variables that increase as microcracking and crushing develop. The yield condition, an extension of Drucker-Pruger model, is based on the yield function proposed by Lubliner et al. (1989) and incorporates the modifications proposed by Lee and Fenves (1998) to account for different evaluation of strength under tension and compression. The *CONCRETE COMPRESSION HARDENING and *CONCRETE TENSION STIFFENING options were used to define the stress-strain curve in compression and cracking and postcracking properties for concrete in tension. In the first case, the following uniaxial stress-strain curve, proposed by EC2 (1999) was used:

$$\frac{\sigma_c}{f_c} = \frac{(k\eta - \eta)^2}{[1 + (k-2)\eta]} \qquad (1)$$

where $\eta=\varepsilon_c/\varepsilon_{c1}$, ε_{c1} is the peak strain, assumed equal to $2.9\text{x}10^{-3}$, and k= 1.1 Ec ε_{c1}/f_c.

As far as concrete in tension is concerned, the tensile behavior was assumed to be linear up to the tensile strength. The post-peak behavior, particularly important when fibers are present in the matrix, was calculated according to the Italian Standard (2003), which requires fracture mechanic four point bending tests (4PBT) on beam specimens (150x150x600 mm). Figure 7 illustrates the experimental load-displacement curves (CMOD: crack mouth opening displacement) and the geometry of the 4PBTs carried out: four beams were cast with 45/30 fibers while three with 80/30 fibers. In order to find a tensile stress-opening fracture constitutive relationship after the peak stress, numerical analyses were performed using

the FE program MERLIN (Reich et al. 1994), which is based on a discrete crack approach. Figure 8 shows the specimen mesh chosen. The FE Program MERLIN considers the structure as many linear elastic subdomains, linked by interface elements that simulate the cracks, whose position must be known a priori. Interface elements initially connect the subdomains (as rigid links) and start activating (i.e. cracks start opening) when the normal tensile stress at the interface reaches the tensile strength of the material. Afterwards, the crack propagates and cohesive stresses are transmitted between the crack faces according to a stress-crack opening (σ-w) law (which is given as input for the interface elements). Figure 7 shows also the numerical response of the 4PBT indicating a close agreement with the experimental results. The cohesive laws calibrated with MERLIN were reduced to cohesive stress-strain relationships by dividing the fracture opening by a characteristic length value chosen equal to 50 mm (that is the element dimension). These laws were then used as input of *TENSION STIFFENING option of ABAQUS for performing Beam 2 and Beam 3 analyses. The stress-crack opening cohesive laws for 45/30 and 80/30 fibers are reported in Table 3. A hyperbolic softening curve, defined as a multilinear curve, was instead adopted for plain concrete.

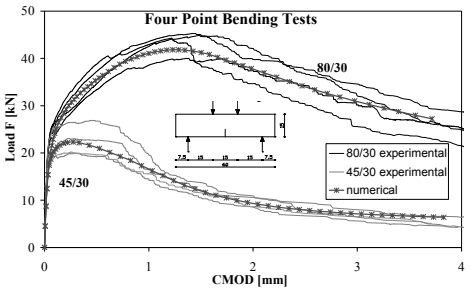

Figure 7. Load-CMOD curves of 4PBT using 45/30 and 80/30 fibers.

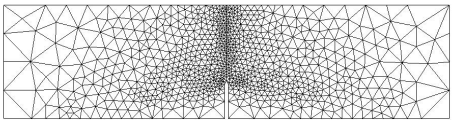

Figure 8. Mesh adopted for 4PBT numerical simulations using MERLIN.

It is finally observed that only the 12 mm thick web panel (1750 mm long) of the prestressed beam specimens was modeled considering concrete nonlinearity, since it was both the predicted shear failure zone in the experiments, and the only beam portion showing macrocracks. Linear elastic concrete was instead assumed in all other portions, leading to a considerable computational time saving.

Table 3. Stress-crack opening-equivalent strain relationships for fiber reinforced concrete.

Concrete type		FIBERS 45/30			FIBERS 80/30		
f_{ct}	MPa	3.96			3.96		
E_c	MPa	35688			34675		
		s	w	ε	s	w	ε
		MPa	μm	E-3	MPa	μm	E-3
		3.96	0.0	0	3.96	0.0	0.0
		2.7	0.02	0.4	3.6	0.05	1
		2.2	0.2	4	4.6	0.4	8
		0.7	0.8	16	4.5	0.7	14
		0.4	1.2	24	3.5	1.0	20
		0.15	2.5	50	2.5	1.5	30
					1.0	3.0	60

3.2 *Reinforcement*

Based on experimental results on cables, a modified Ramberg-Osgood polilinear curve, suitable for low relaxation steel, was defined for prestressing steel. Stirrups, welded wire mesh, and deformed bars were defined as an elasto-plastic materials with hardening by means of a multilinear stress-plastic strain curve representing the actual response of tested bars. Young's modulus was taken equal to 195 000 MPa for pretensioning steel while a value equal to 206 000 MPa was assumed for ordinary steel reinforcement. Table 4 shows the yielding stress, the ultimate stress and strain of each type of reinforcement. Poisson ratio was assumed equal to 0.3 for all kind of reinforcement.

Table 4. Mechanical properties of reinforcing steel.

REINFORCEMENT	f_{sy}	f_{su}	ε_{su}
	MPa	MPa	MPa
P/S CABLES	1674	1860	0.0114
LONGITUDINAL DEFORMED BARS	530	610	0.075
STIRRUPS Φ6	481	614	0.075
MESH Φ5	575	658	0.025

4 COMPARISON BETWEEN FEA AND EXPERIMENTAL RESULTS

Likewise the experimental tests, the numerical analyses were performed with a displacement controlled procedure, by imposing an increasing displacement to the nodes located at the middle of the steel plate transferring the load to the concrete beam. Due to the strongly non-linear behavior of

the tested beams, Regular and Modified Newton-Raphson methods showed deficiency in stability and convergence. Different numerical strategies were therefore used. At first a Modified Riks integration method was adopted. Riks method did not unfortunately succeded in reaching convergence in all cases. In fact, due to the particular geometry and the small cracked area in the tested beams, a localized unstable mechanism developed. In such cases, there is a local transfer of strain energy from one part of the model to neighboring portions, and global solution methods may not work. In this case, ABAQUS provides an automatic mechanism for stabilizing unstable quasi brittle problems through the automatic addition of volume-proportional damping to the model. The *STABILIZE parameter was used for this aim and was calibrated so that the added fictitious viscous forces would be sufficiently high to prevent abrupt collapses and small enough to marginally affect the overall response of the model. A damping factor equal to $5x10^{-5}$ was chosen, as it was small enough to prevent both numerical instability and force overestimation.

Figure 9 illustrates the load-displacement curves for the three Beams in TZ zone and DZ zone, respectively, with the displacement measured at the load location. Note that three identical experimental tests were carried out on Beam type 2, on DZ zone. In all cases, the linear behavior is closely captured by the numerical model. The first cracking point, corresponding to the onset of non-linearity, is similar to the experimental one, particularly in TZ zone tests. As far as post-cracking is concerned, the experimental global response was always more resistant and ductile than the numerical one. This is particularly evident in the three DZ tests. Moreover, the numerical analyses showed a strongly unstable behavior in each of those tests after the first cracking load. This initial numerical instability is related to the lack of any kind of transverse reinforcement (except the minimum required in Beam1) generating the main resisting contributions at early crack stages.

Even if the numerical model initially involves a greater damage amount than the evidence, the model is still capable of capturing the main features of the experimental behavior. In fact, the slope of the post-peak numerical branch is similar to the experimental one. The numerical analyses where not able to reach convergence, hence collapse was assumed, for a global deflection equal to 12÷14 mm, approximately three times higher than deflection at first cracking. For Beam 3 in the DZ zone, although the experimental response was quite stable, ABAQUS was not able to converge beyond a displacement equal to approximately 7mm, even adopting a really small displacement increment and a greater damping factor.

In TZ zone (“transfer length”), due to the presence of shear reinforcement, the numerical response of the Beams appeared to better represent the experimental behavior. The peak load is in all cases very close to the experimental evidence, and the gap between numerical and experimental response is smaller compared to the results of DZ zone. The behavior after cracking appeared to be extremely brittle also in this case, although less damage than in DZ tests was observed. In all case, the slope of the post-peak numerical response is sufficiently similar to the experimental one.

The chosen numerical model is therefore capable of representing the linear and non-linear behavior of the beams tested under shear loading. It is also able to model with sufficient accuracy the fiber contribution to tension softening. The damaged plasticity model is definitely more stable in presence of reinforcing transverse steel, whereas with fibers alone or with light transverse reinforcement it does not capture accurately the immediate post-cracking behavior, leading to underestimations of the structural response and, sometime, to convergence problems.

Figure 10 illustrates the comparison between the numerical and experimental crack pattern in the case of Beam 1, DZ zone. The picture is referred to the structure immediately after first-cracking (point A, Figure 9.b). It is noted that the inclination of the principal tension strains (41° inclined to the horizontal) significantly differs from the experimental crack pattern (the main crack is inclined 23° to the horizontal axis).

This difference is greater in the DZ zone tests and becomes larger at higher loads. In fact, the experimental beams initially showed a diffused crack pattern in the panel, which later developed through a progressive crack rotation and cracks merging together, leading to a single macro-crack oriented as the panel diagonal. This rotation lead to an ultimate resisting mechanism governed by arc action and concrete residual compressive strength.

The numerical model, remaining approximately constant the inclination of the principal tensile strains (still 41° at point B of Fig. 9b), is not able to capture this phenomenon. The inability of the model in rotating the principal tensile strain pattern is most likely the reason of the convergence problems that caused the premature termination of the numerical analyses.

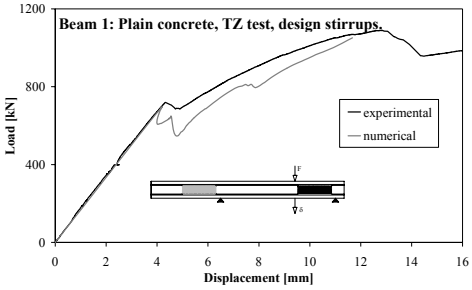

(a)

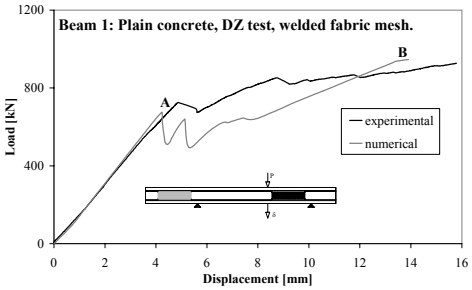

(b)

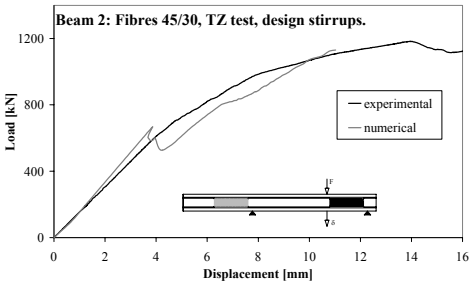

(c)

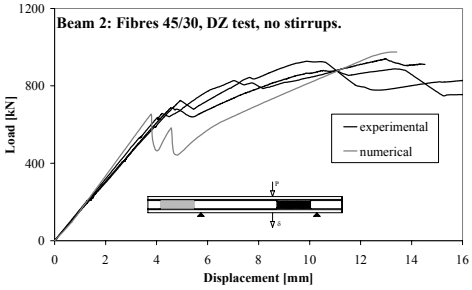

(d)

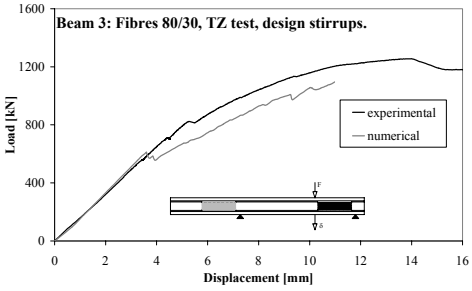

(e)

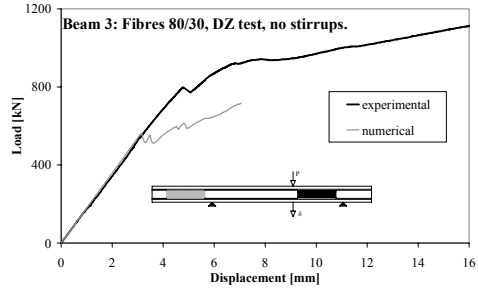

(f)

Figure 9. Numerical and experimental load-displacement curves.

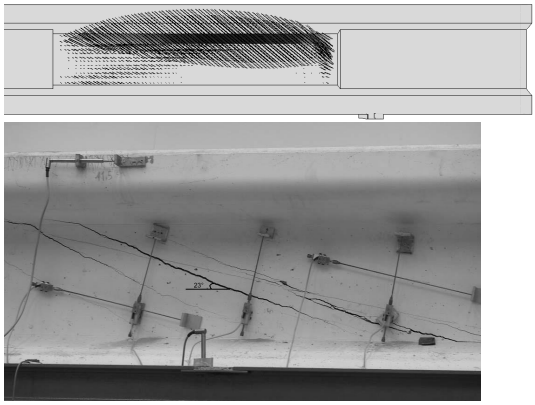

Figure 10. Numerical and experimental crack pattern development, Beam 1, DZ test.

Figure 11 shows a comparison between the numerical and experimental crack opening of Beam 1, DZ zone. The main experimental crack opening was measured by means of potentiometric Penny & Giles transducers (six transducers, indicated in Fig. 11 as "TPT#"). The numerical estimate of the crack opening ("TPT Numerical" in Fig. 11) was derived by averaging the tensile deformations calculated at the Gauss Points closest to the transducer extremities, and by multiplying the average tensile deformation value by the transducer length

It is noted that the numerical crack opening is close to the experimental evidence at early loading stages, while the experimental opening is much higher than the numerical one at later loading stages, closer to the beam failure. This is due to the smeared crack approach adopted by ABAQUS, which is not able to correctly represent crack localization phenomena, thus leading to a higher number of cracks with smaller openings. In fact, the bigger crack opening in the experimental model is due to the progressive formation of a single macrocrack, resulting from the rotation and merging of several smaller cracks.

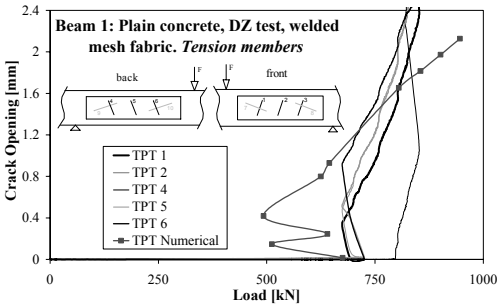

Figure 11. Numerical and experimental crack opening in the panel experimental area.

5 CONCLUSIONS

In this paper, a comparison between numerical analyses and shear experiments on full scale prestressed concrete and fiber reinforced concrete beams are presented.

The analyses were performed using ABAQUS V. 6.3 adopting a 3D solid model in which the section variation along the span, bond between prestressing strands and concrete, and the non-linear behavior of the materials were considered. A damaged plasticity model was adopted for concrete.

The adopted model accurately predicted the post-cracking response of the members in terms of strength and ductility. It was able to simulate the post-peak behavior up to displacements three times higher than the cracking point displacement, where the damage of the structure was really high.

The model resulted more stable in presence of transverse reinforcing steel, while with steel fibers alone or light transverse reinforcement the response appeared to be excessively unstable, particularly immediately after the first cracking load, leading to underestimations of the structural response and, sometime, to convergence problems. Moreover, the model was not able to simulate the final collapse mechanism of the beams, related to arc action, which involved cracks rotation and merging.

However, the shear contribution due to fibers and regular reinforcement, even if underestimated, was modeled with sufficient accuracy.

The numerical analyses, as well as the experimental results, demonstrated that the minimum shear reinforcement may be effectively substituted with steel fibers, resulting in a reduction of labor cost due to the elimination of handling and placing of reinforcement.

Based on the results of the analyses presented, it is possible to conclude that the adopted model can be used to further study the behavior of FRC beams, with the aim to better understand the mechanisms governing shear failure in fiber-reinforced prestressed concrete beams and to develop a practical design procedure to account for the effects of fibers on beam behavior.

6 ACKNOWLEDGEMENTS

The support of Ing. Paolo Magnetti and Ing. Claudio Failla (Magnetti Group, Italy) is gratefully acknowledged as well as the help of Ing. Luca Cominoli and Ing. Sonia Piazzani for the assistance in running the analyses and data processing.

7 REFERENCES

Casanova, P., Rossi, P. & Schaller, I. 1997. 'Can steel fibers replace transverse reinforcement in reinforced concrete beams?', *ACI Material Journal*, 94, 341-354,.

EUROCODE 2 1993. Design of Concrete Structures, UNI-ENV 1992-1-2.

EUROCODE 2 1999. Design of Concrete Structures, prEN 1992-1-:2001.

HKS, 2002. 'ABAQUS V.6.3.1 Theory and Users Manuals,' Providence, Rhode Island.

Lee, J., & Fenves, G. L. 1998. 'Plastic-Damage Model for Cyclic Loading of Concrete Structures,' *Journal of Engineering Mechanics*, vol. 124, no. 8, pp. 892-900.

Lubliner, J., Oliver, J., Oller, S., & Oñate, E. 1989. 'A Plastic-Damage Model for Concrete,' *International Journal of Solids and Structures*, vol. 25, no. 3, pp. 229-326.

Meda, A., Minelli, F., Plizzari, G.P. & Failla, C. 2002. "Experimental study on shear behavior of prestressed SFRC beams"; *6th International Symposium on High Strength/High Performance Concrete, Lipsia, June 16-20 2002*, Vol 1, 369-382.

Meda, A. & Plizzari, G.A. 2003. 'A new design approach for SFRC slabs on grade based on fracture mechanics', *ACI Structural Journal*, (2003). Accepted for publication.

Padmarajaiah, S.K. & Famaswamy, A. 2002. 'A finite element assessment of flexural strength of prestressed concrete beams with fiber reinforcement', *Cement and Concrete composites Journal*, 24, 229-241.

Paramisan, P., Kiang-Hwee, T. & Murugappant, K. 1995. 'Finite element analysis of partially prestressed steel fiber reinforced beams in shear', *Elsevier Advanced Cement Based Material Journal*, 2, 231-239.

Reich, R., Cervenka, J., & Saouma, V.E. 1994. 'MERLIN, a three-dimensional finite element program based on a mixed-iterative solution strategy for problems in elasticity, plasticity, and linear and nonlinear fracture mechanics', *EPRI, Palo Alto (CA).*

UNI 11039 2003. 'Steel fiber reinforced concrete - Part I: Definitions, classification specification and conformity - Part II: test method for measuring first crack strength and ductility indexes'*, Italian Board for Standardization*.